CERN-ACC-2015-0016

HiLumi LHC

FP7 High Luminosity Large Hadron Collider Design Study

Deliverable Report

SPS Test Prototype Cryomodule

Brodzinski, K (CERN) *et al*

30 January 2015

The HiLumi LHC Design Study is included in the High Luminosity LHC project and is partly funded by the European Commission within the Framework Programme 7 Capacities Specific Programme, Grant Agreement 284404.

This work is part of HiLumi LHC Work Package **4: Crab cavities**.

The electronic version of this HiLumi LHC Publication is available via the HiLumi LHC web site <http://hilumilhc.web.cern.ch> or on the CERN Document Server at the following URL: <http://cds.cern.ch/search?p=CERN-ACC-2015-0016>

Grant Agreement No: 284404

HILUMI LHC

FP7 High Luminosity Large Hadron Collider Design Study

Seventh Framework Programme, Capacities Specific Programme, Research Infrastructures, Collaborative Project, Design Study

DELIVERABLE REPORT

SPS TEST PROTOTYPE CRYOMODULE

DELIVERABLE: D4.3

Document identifier:	HILUMILHC-Del-D4-3
Due date of deliverable:	End of Month 38 (December 2014)
Report release date:	30/01/2015
Work package:	WP4: Crab Cavities
Lead beneficiary:	CERN
Document status:	Final

Abstract:

The two-cavity prototype crab cavity cryomodule conceptual design towards the SPS beam tests is described in detail including the functional requirements, dressed cavity design, thermal and magnetic shielding and the outer vacuum vessel with all relevant interfaces. Mechanical and thermal studies where relevant are also described.

The HiLumi LHC Design Study is included in the High Luminosity LHC project and is partly funded by the European Commission within the Framework Programme 7 Capacities Specific Programme, Grant Agreement 284404. HiLumi LHC began in November 2011 and will run for 4 years.

Delivery Slip

	Name	Partner	Date
Authored by	K. Brodzinski, O. Capatina, A. Macpherson S. Pattalwar, T. Jones	CERN STFC	30/11/2014
Edited by	R. Calaga, C. Noels G. Burt	CERN ULANC	30/11/2014
Reviewed by	R. Calaga,WP4 coordinator G. Burt, WP4 co-coordinator L. Rossi, Project coordinator	CERN ULANC CERN	27/01/2015
Approved by	Steering Committee		30/01/2015

TABLE OF CONTENTS

Executive summary

The two-cavity prototype crab cavity cryomodule conceptual design foreseen for the SPS beam tests is described in detail. This includes the functional requirements, dressed cavity design, frequency tuner, HOM couplers, thermal and magnetic shielding and the outer vacuum vessel with all relevant interfaces. Mechanical and thermal studies where relevant are also described.

1. INTRODUCTION

To reach the goal of $(200 \ldots 300)\ \mathrm{fb}^{-1}$ per year with the LHC, stronger focussing to reach smaller beam sizes and non-zero crossing angles are studied in HiLumi LHC; the geometry of such beams however require crab cavities to realign the bunches in the interaction point (IP) for maximum overlap. A pair of crab cavity structures placed on either side of a high-luminosity interaction region (IR), separated by an integer multiple of half the betatron period, will create a head-tail rotation around the bunch barycenter – localized to the IR – for the head of each bunch to one side, for the tail to the other side.

Since crab cavities of such type have never been realized and used with hadron beams, beam tests with a prototype two-cavity cryomodule is a pre-requisite to identify potential risks of the technology for the LHC [1]. Therefore, an essential milestone for a crab cavity test in the SPS is planned to demonstrate the reliable operation, machine protection, cavity transparency and to understand the long term effects on hadron beams. All RF manipulations and cavity-beam interactions will be first validated and commissioned in the SPS with a prototype two cavity crab cavities system. This is anticipated to be performed in 2017-18.

A series of complex boundary conditions has made the design of cryomodule and particularly the helium vessel extremely challenging. A preliminary analysis [2] was undertaken to develop a concept cryomodule to provide open access to internal components with the cavity string loaded from a side as shown in Figure 1.

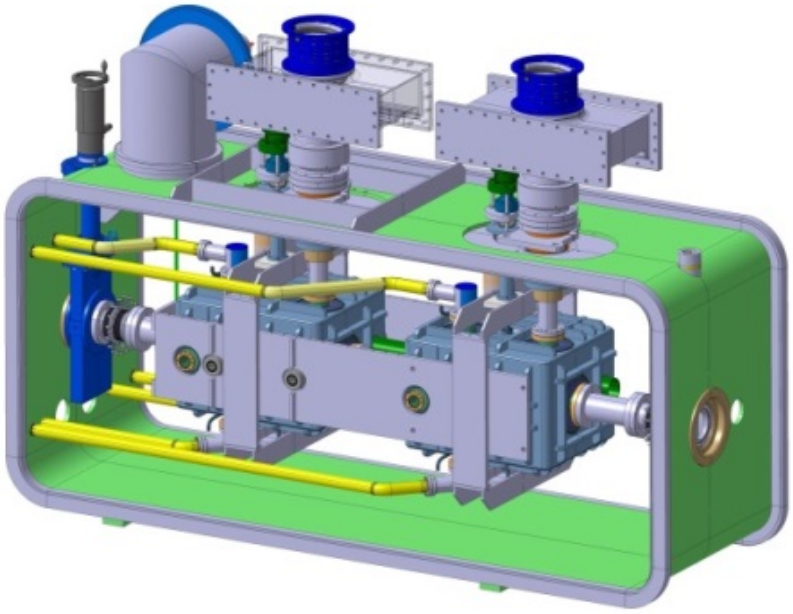

Figure 1: *Side loaded, open access cryomodule for the SPS tests*

This document summarizes the progress towards developing a prototype of the two-cavity cryomodule towards the SPS beams for two cavity types under consideration. The cryomodule consists of two dressed cavities with their respective main coupler, multiple HOM couplers (2-4 per cavity), tuning system, magnetic and thermal shielding, vacuum vessel and all the internal and external interfaces. Relevant mechanical and thermal studies are described to comply with the pressure loading conditions as specified by the functional specifications [3].

2. FUNCTIONAL REQUIREMENTS

2.1. INTERNAL BOUNDARY CONDITIONS

2.1.1. Operating Temperature

The BCS resistance of Niobium at 4.5 K and 400 MHz is around 50 nΩ, which is more than 10 times larger than the value at 2 K. The complex shapes of the cavities may also be susceptible to microphonics caused by LHe boil-off, hence operation below the lambda point with He II is preferred. For these reasons operation at 2 K is baseline. This will require the provision of saturated He II at about 2 K to the crab cavity location in LHC. The current heat load limits for LHC are not currently known, but is likely to be around 3 W of dynamic load per cavity at 2 K.

2.1.2. Cavity Geometry and Interfaces

Following the recommendation of the May 2014 technical review [4], only two cavity designs are considered for the engineering design towards the SPS tests (DQW [5] and RFD [6]). The mechanical design of the cavities ensures their safe use under maximum loading condition during its entire life-cycle. The cavity was dimensioned to cope with several mechanical constraints: ensure elastic deformation during maximum pressure as well as during all transport and handling conditions; maximise tuning range; minimise sensitivity to pressure fluctuation; avoid buckling due to external pressure; maximise the frequency of the first mechanical natural mode. The final mechanical design of the cavities including all external interfaces is shown in Figure 2.

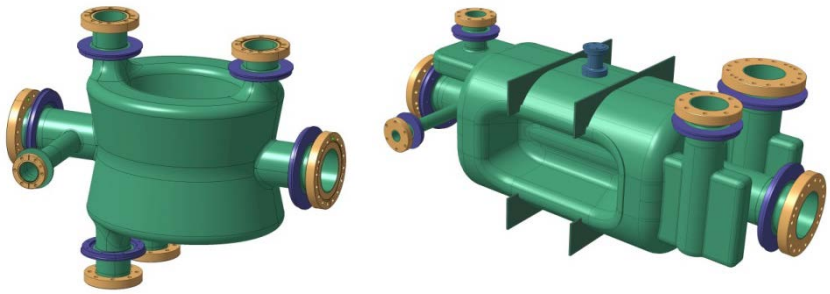

Figure 2: Schematic view of the cavity with interfaces (left: DQW & Right: RFD).

2.1.3. Magnetic Shielding

Assuming a cavity geometric factor of $G \approx 100\ \Omega$, the additional surface resistance due to trapped flux R_{mag} is required to be below $(1 \div 2)\ \text{n}\Omega$ to stay in the shadow of the total surface resistance specification of 10 nΩ. To achieve this, magnetic shielding in the cryostat should reduce the external magnetic field on the outer surface of the cavity by at least a factor 100 (reaching $< 1\ \mu\text{T}$ assuming the earth magnetic field. Note that ambient magnetic field in the SPS due to the bus bars are much higher than the assumed earth's magnetic field [7].

2.1.4. Frequency Tuning

For beam tests in the SPS a slow mechanical tuner system is required to bring the cavity on resonance in the energy range of the SPS (±60 kHz). In addition the tuner in conjunction with the RF feedback should allow for detuning or retuning of the cavity at a safe frequency, including cavity transparency and the suppression of the coupled bunch instabilities. Table 1 below summarizes the potential energies at which SPS can be operated for crab cavity tests and their corresponding RF frequencies compared to that of the LHC operation.

Table 1: Detuning ranges for the LHC and SPS

Parameter	Unit	LHC	SPS		
Energy	GeV	450…7000	120	270	450
Frequency	MHz	400.79	400.73	400.78	400.79
ΔF_0	kHz	0	-58.2	12.2	-2.4
Bandwidth	kHz	0.4…4	0.4…4	0.4…4	0.4…4
Detuning	kHz	±5.5	±21.7		

The largest detuning in the LHC is expected to a maximum of ±5.5 kHz or below in the LHC and approximately ±21.7 kHz in the SPS. The detuning requires a resolution of at least ¼ of the final cavity bandwidth due to available power limits. Additional studies have to be carried out to verify if a tuning speed higher than the mechanical tuner is required if limitations arise from feedback and/or orbit control.

2.2. EXTERNAL BOUNDARY CONDITIONS

2.2.1. Space Availability

The volume of the crab cavity installation is composed of the crab cavity cryomodule, two RF power amplifiers, a support table on which cryomodule and RF power are mounted, a cryogenic coldbox, 2 helium pumps, and 4.5 K dewar reservoir, cryogenic distribution valve box with interconnection transfer lines and mechanical beam line infrastructure and instrumentation. In short, the crab cavity installation occupies ~80% of the ground level of the SPS LSS4 alcove.

The total cryomodule envelope based on the cross section taken from the SPS test prototype design would be 1.05 x 2.15 m^2 (width x height from the floor to the upmost part, 1.2 m above the beam axis). Power and cryogenic connections to the cryomodule come from the top, so space directly above the cryomodule is also required. The length of the cryomodule is

dependent on the cavity type with the longest cavity in a two-cavity configuration measuring a total of 2.9 m without including the external warm gate valves. Gate valves are foreseen at each end of the cryomodule, and additional gate valves exist around mechanical switching of the beam line.

In the LHC, the available total length is 13.4 m for 8-cavities per side of the interaction region for both beams including gate valves. This is compatible with the 2-cavity cryomodule configuration as for the SPS module. Therefore, the SPS tests also serve as an important integration validation test.

The SPS ring is equipped in LSS4 (41737, presently used for the COLDEX experiment) with a special bypass (Y-chamber) with mechanical bellows that allow horizontal displacement. This allows for a test module to be moved out of the beam line during the regular operation of the SPS and only moved in the beam line during the dedicated periods to study the crab cavity test module with beam. This setup is essential both due to aperture limitations of the crab cavities and the risk associated with leaving the cavities in the beam line with different modes of operation in the SPS. The cryomodule is placed on a movable table which can be moved sideways by 510 mm (see Figure 3). A special working group (crab cavity technical coordination) has been set up to follow up the various integration issues including the RF and cryogenic systems.

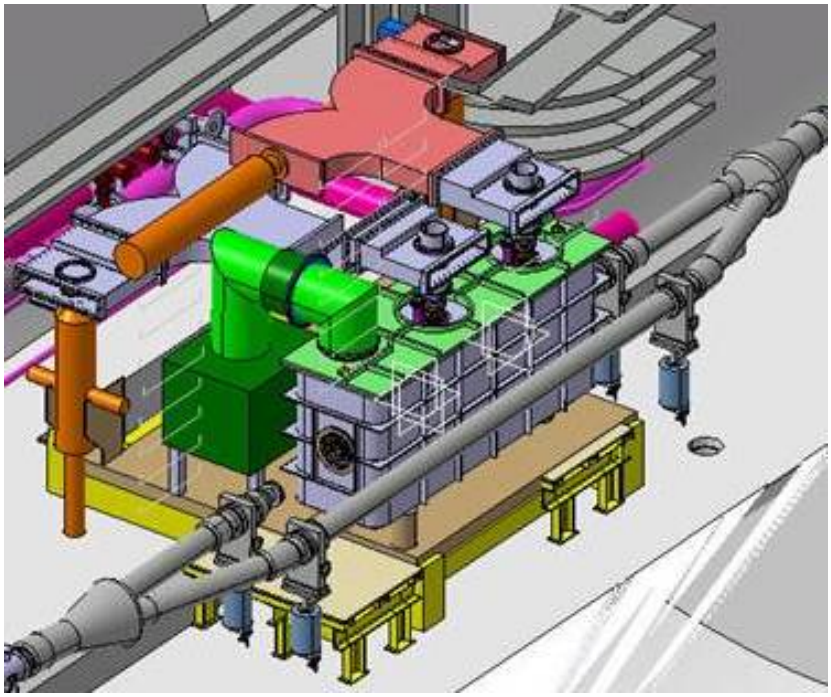

Figure 3: 3D integration of the cryomodule, RF assembly and the cryogenics in the SPS [7].

The relevant cryomodule envelope dimensions for the SPS tests are summarized in Table 2. In general, the SPS constraints are tighter than those of the LHC.

Table 2: Cryomodule envelope dimensions

Description	**[mm]**
Cryomodule length (gate-valve to gate-valve)	3000
Horizontal distance cavity axis to inner edge of cryomodule volume	420
Vertical distance floor to cavity axis	1200
Maximum height above cavity axis	1200
Inner diameter of cavity beam pipe	84
Horizontal distance cavity axis to bypass beam pipe axis	510

2.2.2. Y-chamber and Movable Table

The size of the cryomodule required an enlargement of the mechanical by-pass Y-chamber from the existing 12°to 16°opening angle. Figure 4 show the design evolution from the Y-chamber design to allow for the increased opening angle without any increase of impedance due to the reduced aperture.

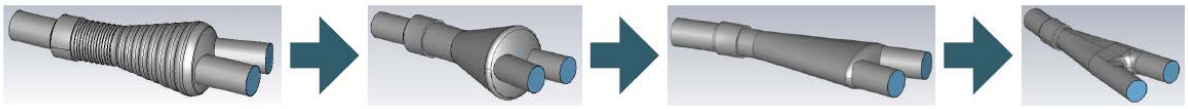

Figure 4: The Y-chamber design evolution for the crab cavity module to allow for an transverse movement of approximately 510mm and reduced impedance [7].

2.2.3. RF Infrastructure

Specially designed WR2300 will feed the RF power from the Tetrode amplifiers to the respective cavity (see Figure 5). Placement of the amplifiers on the movable table will depend on the full integration of the cryomodule, transmission lines and circulator. An LHC type circulator, although over-dimensioned, is preferred for reasons of maintenance and spare policy. A 3D integration of the cryomodule and the RF assembly in the LSS4 region is shown in Figure 5.

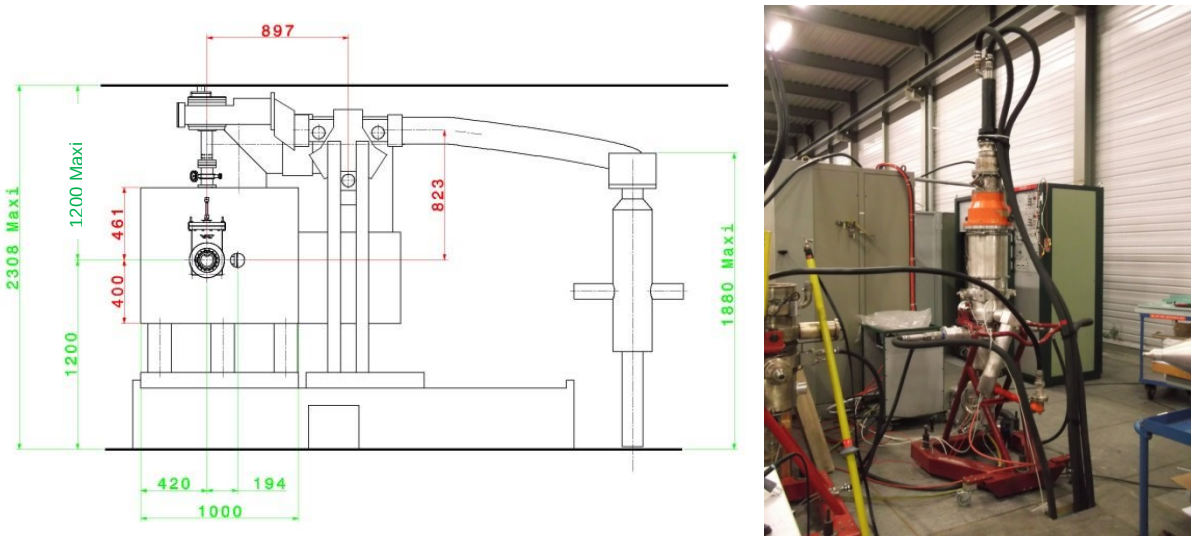

Figure 5: Cryomodule and RF system layout in the LSS4 cavern (left) and a 400 MHz Tetrode amplifier under test (right).

In the LHC, the 4 cavities per IP side are always powered on tune, initially with a small voltage (10-15% of the nominal) and counter-phased, with active feedback to guarantee maximum beam stability during the entire cycle. Therefore, beam injection with counter-phased cavities with low voltage requires testing in the SPS. Other issues related to beam loading and transient effects with and without RF feedback and slow orbit control will be studied to evaluate the stability and tolerances required from the feedback systems. Induced RF trips and their effects on the beam will be studied in detail to guarantee machine protection and to devise appropriate interlocks. Long term effects with crab cavities on coasting beams at various energies will also be tested.

3. CRYOGENICS

3.1. CRYOGENIC SERVICES

At present, the SPS-LSS4 region is equipped with the TCF20 cryogenic box. It was originally planned to upgrade the existing cold box to deliver 2 K Helium for the operation of the crab cavities. Due to the very limited capacity available in the SPS TCF20 refrigerator, the total losses (static and dynamic) are limited to a maximum of 25 W (at 2 K). The heat load of the two-cavity cryomodule, however conservative, is at least 15% higher than the TCF20 capacity. A replacement for the TCF20 to increase the capacity to approximately 40 W is planned to be put in place for the SPS tests [8]. Despite the plan to increase the capacity, a strong effort is put in place to minimize the heat load of all cavity elements and cryomodule interfaces to ensure a successful beam test in the SPS prior to any installation in the SPS.

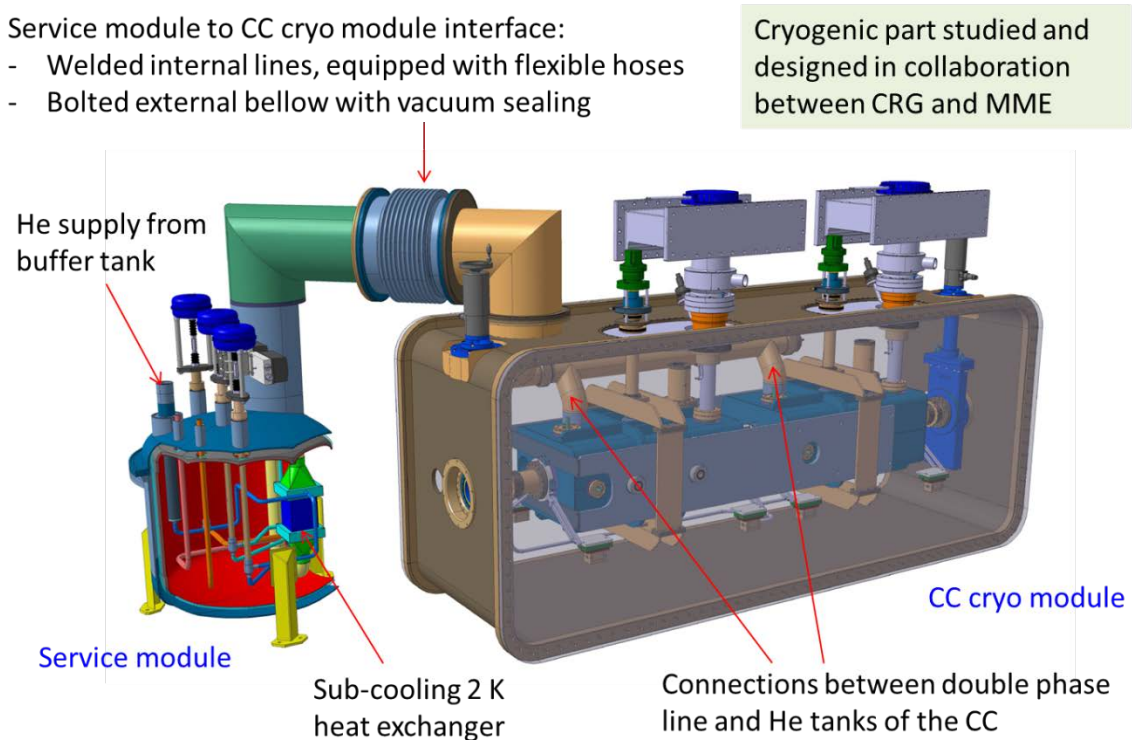

Figure 6: Cryomodule and external cryogenics service module

3.2. COOLING SCHEMATIC

Cryogenic operation of the cryomodule is based on two cooling circuits, one for the operation at 2 K for cavities and the other at 80 K for thermal intercepts and shield using liquid nitrogen [8][9]. The temperature of 2 K is achieved by reducing the vapour pressure of the liquid helium to 30 mbar by a 2-K heat exchanger and warm vacuum pump via an external service module as shown in Figure 6.

Figure 7 shows a schematic for the cryogenics operation of the cryomodule. Represented in yellow helium circuit is split into two loops, one for cool down (bypassing sub-cooling heat exchanger) supplying the cavity helium tank from the bottom and main cooling loop for normal operation with superfluid helium (both supply and return lines are connected on opposite extremities to double phase collector above the cavities helium tank). Thermal shield and the intercepts will be cooled using the liquid nitrogen supplied via the valve box. However, all outlets for nitrogen will be placed on the crab cavity module side and directed to the recovery collector.

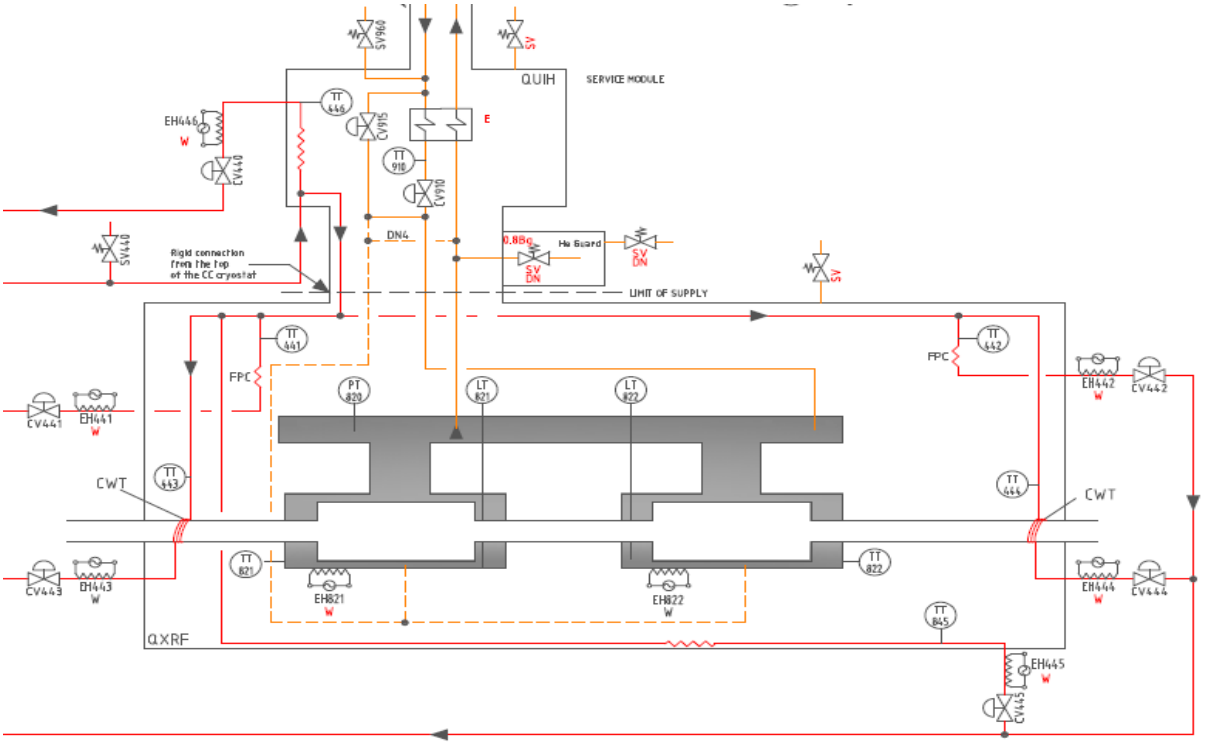

Figure 7: Cooling scheme for the crab cavity module for SPS test.

3.3. THERMAL SHIELDS AND INTERCEPTS

In order to reduce the thermal load on superfluid helium vessels, the cryomodule will be equipped with actively cooled thermal shield operating at 80 K using liquid nitrogen pressurized at 2-3 bar. The thermal shield will be covered with 30 layers of cryogenic multi-layer insulation (MLI).

3.4. HEAT LOAD ESTIMATES

Table 3 shows the estimated contributions to the heat load [10] to the cryogenic circuits at 2 K and 80 K for the two cryomodules. Two different configurations for the HOM couplers are being considered for the RFD cavities.

Table 3: Heat Load Estimates in Watts

	DQW		RFD Coax cables		RFD 1 Coax + 1 Chimney	
Static at >>	2 K	80 K	2 K	80 K	2 K	80 K
Radiation	0.6	35	0.7	35	0.7	35
CWT	3	12.6	3	12.6	3	12.6
Support	0.2	5	0.8	5	0.8	5
FPC	4	100	4	100	4	100
Instrumentation	1	0	1	0	1	0
HOM/ Pick Up	6.4	30	4.4	20	8.8	120
Tuner	0.3	10	0.3	10	0.3	10
Total Static >>	**15.5**	**192.6**	**14.2**	**182.6**	**18.6**	**282.6**
Dynamic						
Cavity	6	0	6	0	6	0
FPC	5.6	10	5	20	5	20
HOM/ Pick up	4.2	10	2.8	10	1.9	10
Beam	0.5	0	0.5	0	0.5	0
Total Dynamic	16.3	20	14.3	30	13.4	30
Total	31.8	212.6	28.5	212.6	32	312.6

4. DESIGN SOLUTIONS AND ANALYSIS

4.1. SAFETY CONSIDERATIONS

The cavities, the helium vessel and the cryomodule will undergo a series of cryogenic tests at SM18 at CERN, followed by complete system tests on SPS. Thermal and mechanical designs of the cavity, helium vessel and all associated components of the cryomodule must satisfy the safety requirements stated by PED and CERN. In principle it is possible to design a cryomodule to the lowest PED category, however the lower limit of 1.8 bar (absolute) that must be assigned to the relief valves as set by SPS requirements has resulted in raising the PED category of the system to 1 or higher, as shown in Figure 8. All the mechanical components have been designed to meet the requirement defined by the category -1 of the pressure vessel code.

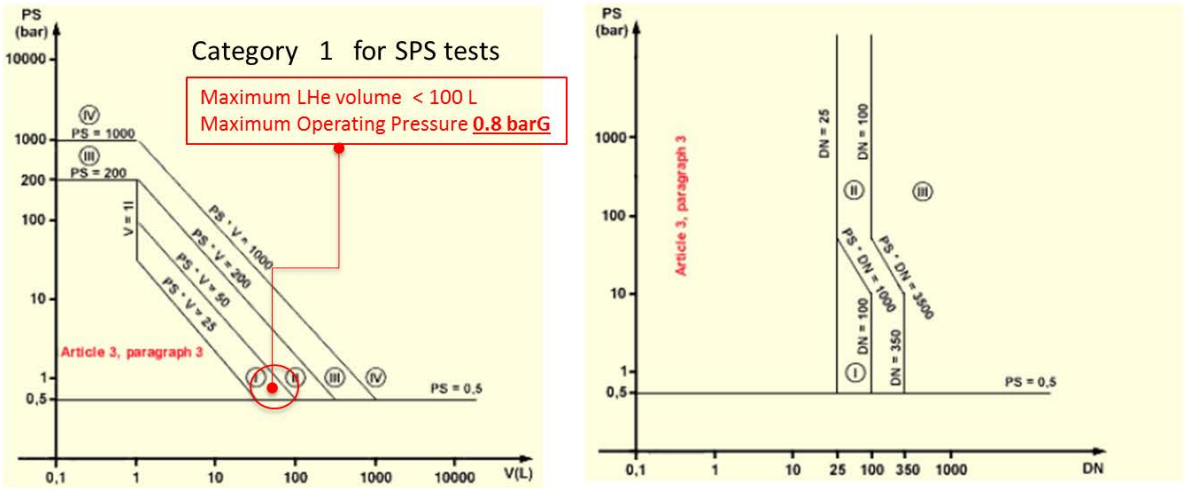

Figure 8: The cryomodule is classified as category-1.

4.2. CAVITY DESIGN AND FABRICATION

The superconducting resonators are fabricated from bulk niobium sheets by electron-beam welding of deep-drawn parts. A final thickness of 4 mm was calculated to be acceptable in order to cope with all the mechanical constraints as well as minimizing the cost of the cavity production. The cavities are bath-cooled by saturated super-fluid helium at 2 K. Each cavity is equipped with: a helium tank, a tuning system, a fundamental RF power coupler, a field probe and two or three HOM couplers. A functional specification including all tolerances for the cavity with its interfaces to develop manufacturing drawings for the DQW and the RFD are shown in Figure 9 and Figure 10 respectively [11]

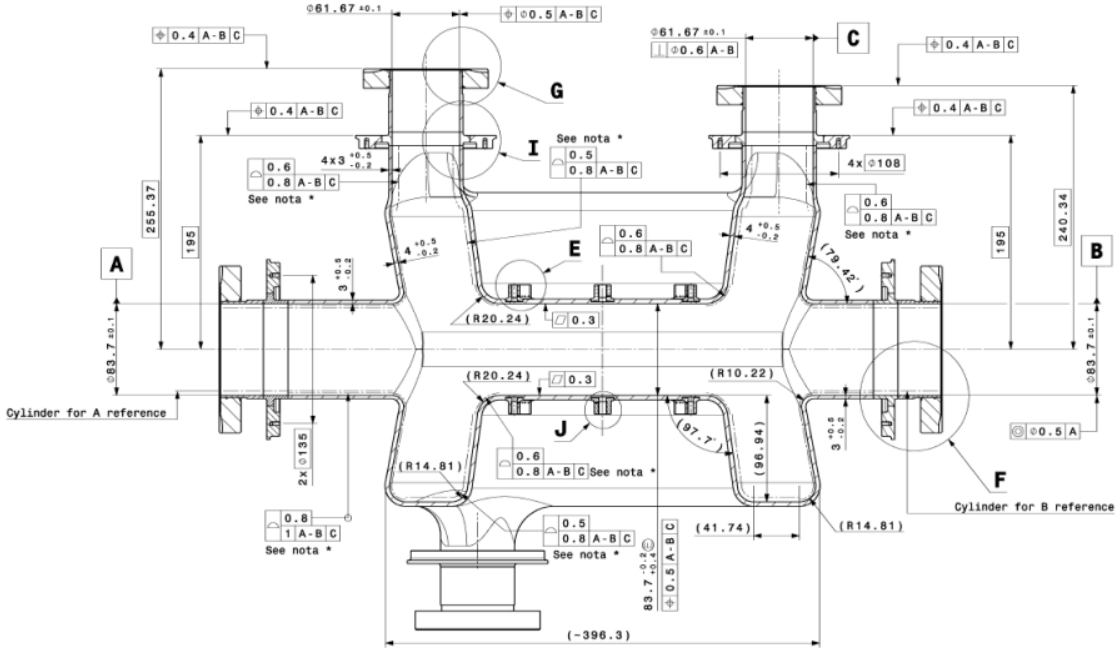

Figure 9: Dimensional plot with tolerances of the DQW cavity

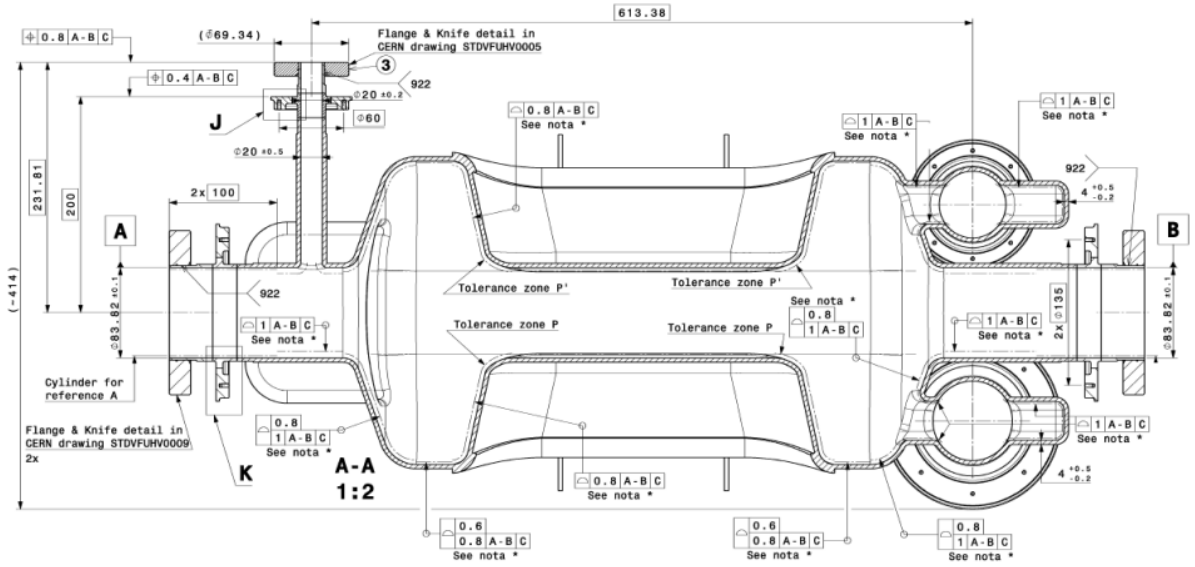

Figure 10: Dimensional plot with tolerances of the RFD cavity

4.3. CAVITY INTERFACE PORTS AND HELIUM VESSEL

The helium tank will contain saturated superfluid helium at 2 K, cooling the cavity and allowing the extraction of the heat dissipated in the cavity and adjacent cold components. Superfluid helium is an excellent thermal conductor for limited heat flux. Above a critical heat flux, the temperature increases drastically and eventually superfluidity is lost. The geometry of the helium tank has been determined to allow this maximum heat extraction while optimising the quantity of the helium to be used [12].

Two choices of material have been studied for the helium tank: stainless steel and titanium. The titanium has the advantage of the same thermal contraction as niobium (in the order of 1.5 mm/m from ambient temperature to 2 K), while the thermal contraction of stainless steel is twice as large leading to larger thermal stresses. The advantage of stainless steel is the manufacturability and the ease of welding due to established techniques thus reduces the overall cost. However, for the unconventional geometries of the crab cavities, titanium grade 2 was chosen as the optimum material for the helium tank, allowing for rigid connections of cavity ports to the helium vessel.

The helium tank has a structural role and its rigid connection to the cavity ports ensures optimum boundary conditions for the cavity during mechanical loading, in particular during maximum pressure loading and tuning. The helium tank geometry was chosen to limit the maximum stress on the cavity to tolerable values [3]. Figure 11 shows a qualitative stress distribution in the cavity wall during maximum pressure. The red colour indicates only small areas of high stress, which is tolerable. This distribution as well as the maximum values is directly influenced not only by the cavity geometry but also by the helium tank configuration.

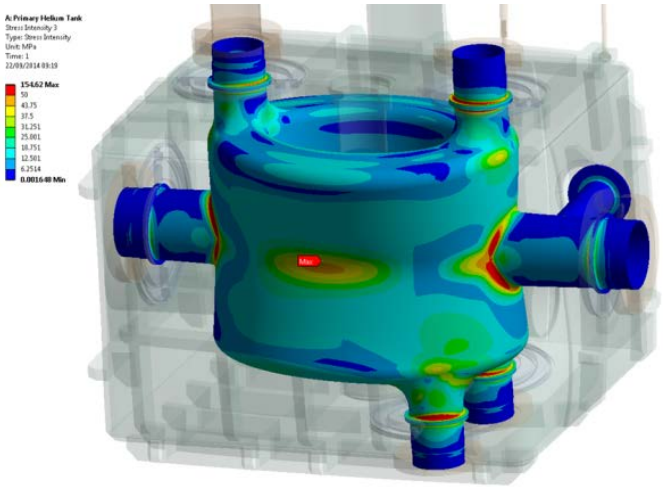

Figure 11: Mechanical stress induced by maximum pressure on the DQW cavity inside its helium tank. Red indicates regions with highest stress, which can be tolerated if confined to small areas.

A major concern for the mechanical design were the transitions from the helium tank to all the adjacent components, in particular the main coupler, HOM couplers, the flanges for connection to the beam pipes and helium pipes. All flange connections are stainless steel to stainless steel connections. Due to its proximity, the second beam pipe had to be integrated inside the helium vessel and consequently will be at 2 K; it is proposed to use a niobium beam pipe.

4.4. DRESSED CAVITY

A schematic view of the DQW and RFD cavities inside their helium tanks and equipped with the required ancillary equipment are shown in Figure 12 and Figure 13.

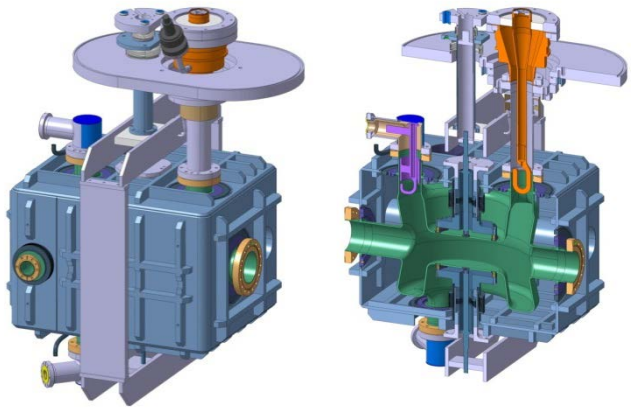

Figure 12: Left: The DQW cavity inside its helium tank with the field probe port (front), beam port (right) and tuner frame around. Right: sectional view of the DQW cavity inside its helium tank with the power coupler (top right, orange), HOM coupler (left, top and bottom) and tuner (centre, top and bottom).

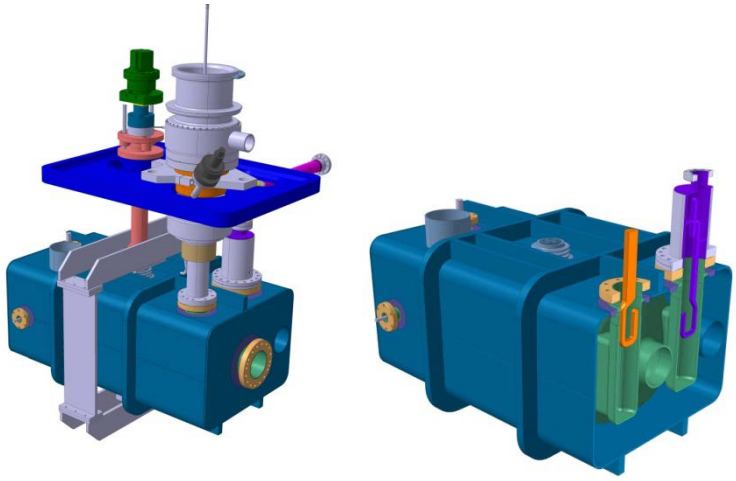

Figure 13: Left: the RFD cavity inside its helium tank with the field probe port (centre left), beam port (centre right), tuner frame around helium vessel and tuner actuation (top centre). Right: Schematic sectional view of the RFD cavity inside its helium tank with the power coupler (orange) and HOM coupler (violet).

4.5. MAGNETIC SHIELDING

The magnetic shielding effect relies upon the natural tendency of the magnetic flux density lines to follow a path where the permeability is highest. In addition it can be shown that the peak flux density in any shielded volume is of the order of the maximum flux density in walls divided by the permeability of the wall material. As the permeability of al ferromagnetic (shielding) materials decreases with the increase of the flux density beyond a certain value the wall thickness must be chosen accordingly in order to avoid saturation and poor shield performance. Another important feature is that the wall thickness necessary to achieve a particular shielding ratio increases in proportion to the increase of shielded volume. In other words larger volumes require thicker walls in order to reduce the external magnetic field to the same level. Very high levels of shielding can be achieved by using carefully engineered multi-layer concentric cylindrical shells and these allow for a significant reduction of the total mass of shielding material at the expense of increasing the total volume occupied by the shield. This solution is implemented in the construction of zero-gauss chambers. Magnetic shielding is further complicated by the presence of apertures necessary to provide access to the shielded object. It should be kept in mind that the magnetic shielding effect is anisotropic in general. The performance of the shield depends upon the orientation of the shield with respect to the external magnetic field. For example a shield in the form of an open cylindrical shell is most effective when the external field is perpendicular to the cylinder axis and least effective when the field is parallel to the axis.

4.5.1. Magnetic Shielding and Analysis

Two shielding solutions for the cryo-module have been considered [13] and the results from the analysis are presented below. The first option is single-layer solution consisting of a box made of 3 mm thick mu-metal sheet. It has been assumed that the external magnetic field is homogeneous and its strength is of the order of the earth's magnetic field. In order to add some contingency 60 μT external field strength has been assumed.

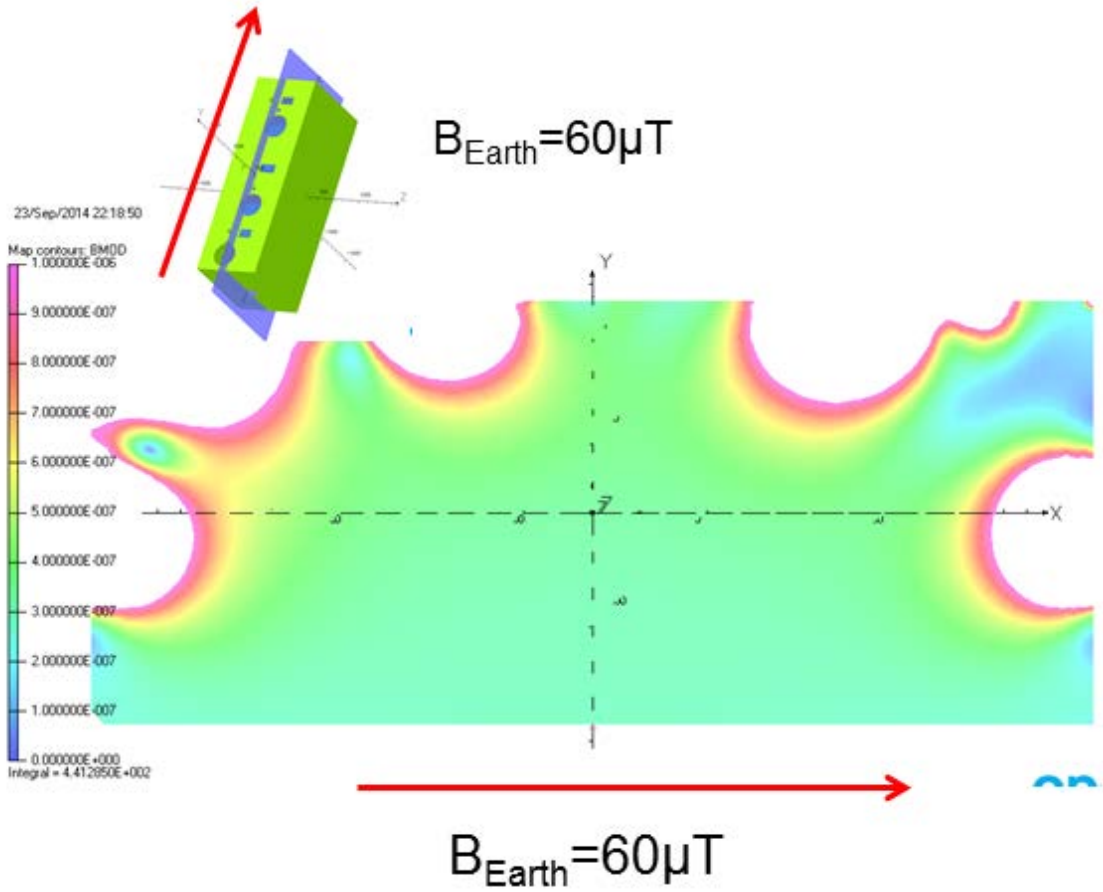

Figure 14: Magnetic flux density inside the single-layer, 3mm thick, mu-metal shield, scale 0 to 1 μT (left). An external field of 60 μT in the direction parallel to X (longitudinal) is used. The inset shows the orientation of the shield with respect to external field and the position of plane where the field is plotted. White areas indicate flux density levels in excess of 1 μT.

The worst case scenario (strongest field inside the shielded volume) is when the external field is parallel to long side of the shield. Figure 14 shows the result. As can be seen the field inside the shielded volume is of the order of 0.5 μT, which is within the specified range (lower than 1 μT). However, this situation does not leave enough safety margin. Shielding performance can be affected by a number of factors that are not easily taken into account in a simulation. A single-layer solution is easier and cheaper to implement (Figure 15), however, it might be susceptible to variation in the magnetic properties of mu-metal, presence of ferromagnetic objects in the vicinity of the shield and stronger fields resulting from unshielded current-carrying conductors. A single-layer solution may prevent further modifications to the apertures.

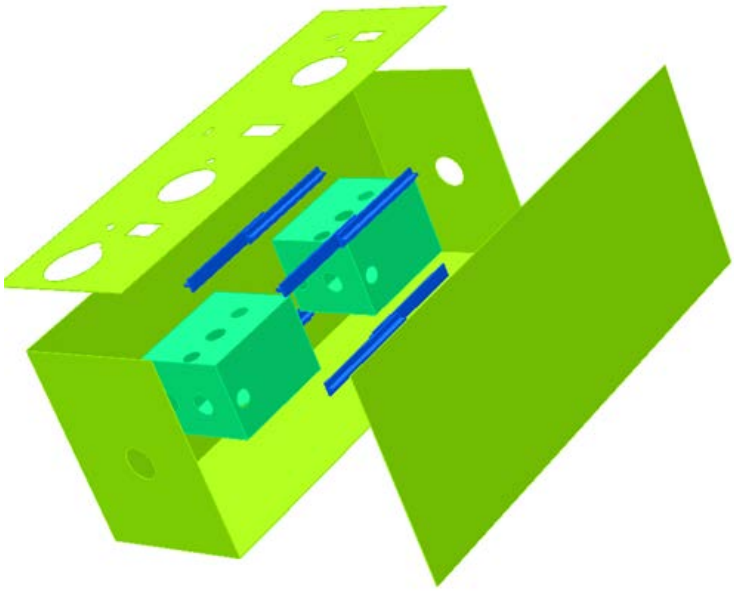

Figure 15: Double-layer magnetic shield design. The outer mu-metal layer is in light green, the two cryoperm vessels are in dark green and the invar rods are in blue.

In order to eliminate this problem a second shielding layer is added around each cavity (Figure 18). As the two inner shells operate at liquid helium temperatures it is necessary to use a suitable material that retains its high permeability at these temperatures, such as 1mm thick Cryoperm or Aperam Cryophy. The invar rods are included in the model in order to make sure that they do not affect the overall performance of the shield. Figure 16 shows the result.

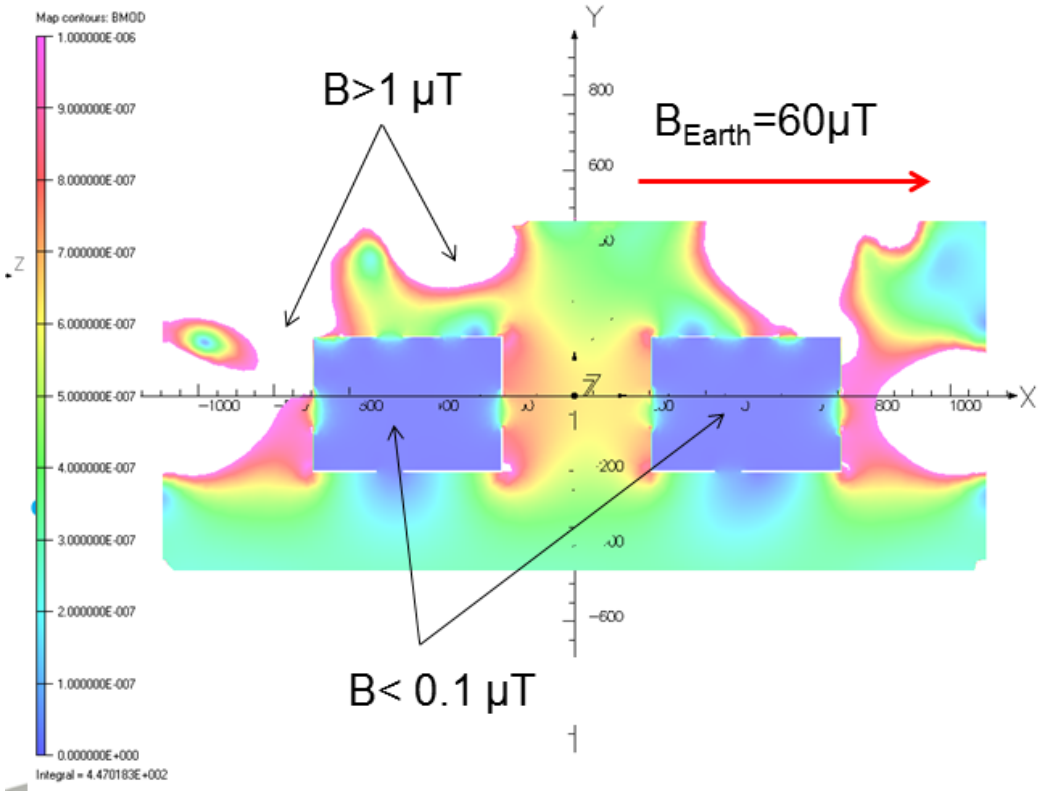

Figure 16 Magnetic flux density inside the double-layer shield,(3mm thick, mu-metal and 1mm thick Cryoperm) , scale 0 to 1 µT (left). An external field of 60 µT in the direction parallel to X (longitudinal) is used.

As can be seen the flux density level inside the Cryoperm vessels is now well below 0.1 µT. The actual field levels are in the nT range and can be assumed zero within the accuracy of the simulation. However, accurately calculating the field at this level is not an easy task as it requires the knowledge of the permeability at very low field strengths. Figure 17 shows the performance of the shield when the external field is horizontal and parallel to the short side of the mu-metal box. As can be seen in this case the external field penetrates the apertures in the mu-metal layer to a much lesser extent, as expected.

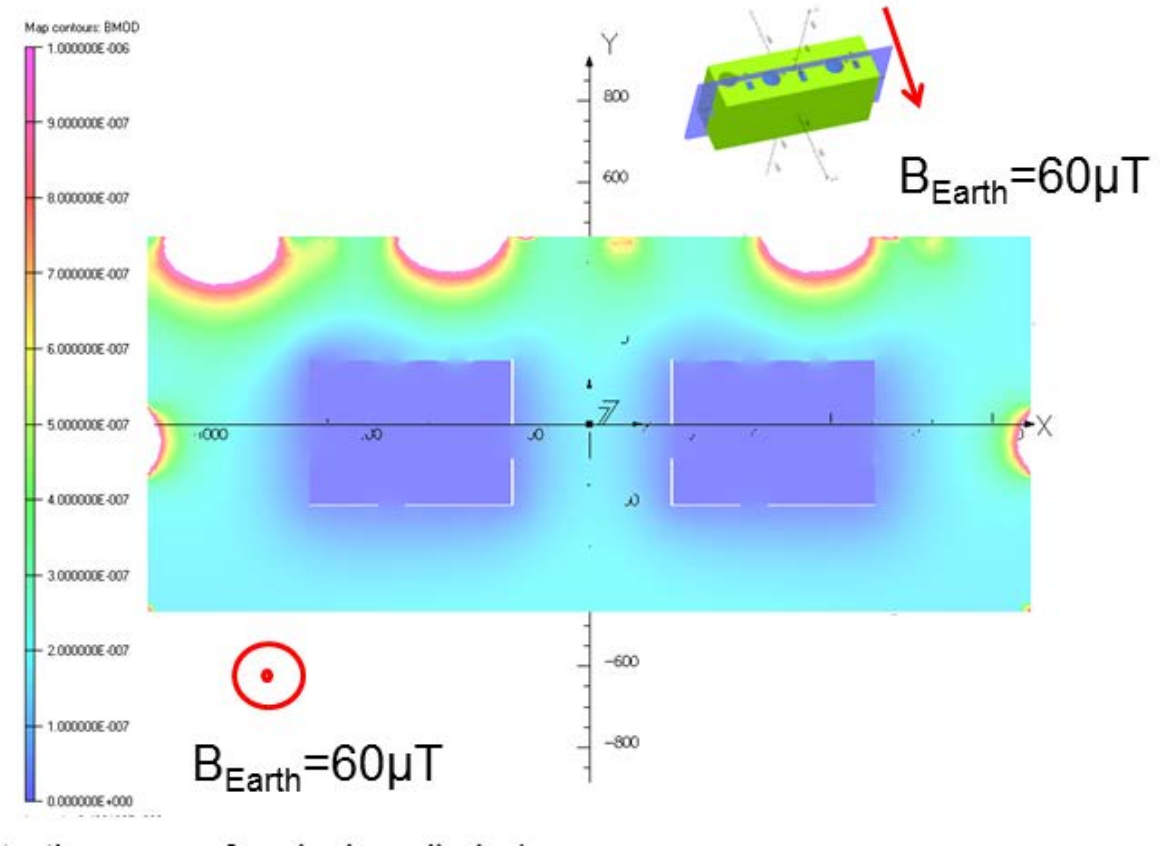

Figure 17: The same as in Fig. 16 but the external field of 60 µT is horizontal and parallel to Z (shown on the inset).

In order to reduce the size of the holes in the internal shield the cold magnetic shielding will be integrated inside the helium vessel [14] as presented in Figure 18. The internal shield is 1 mm thick and will be made from Cryoperm or Aperam Cryophy.

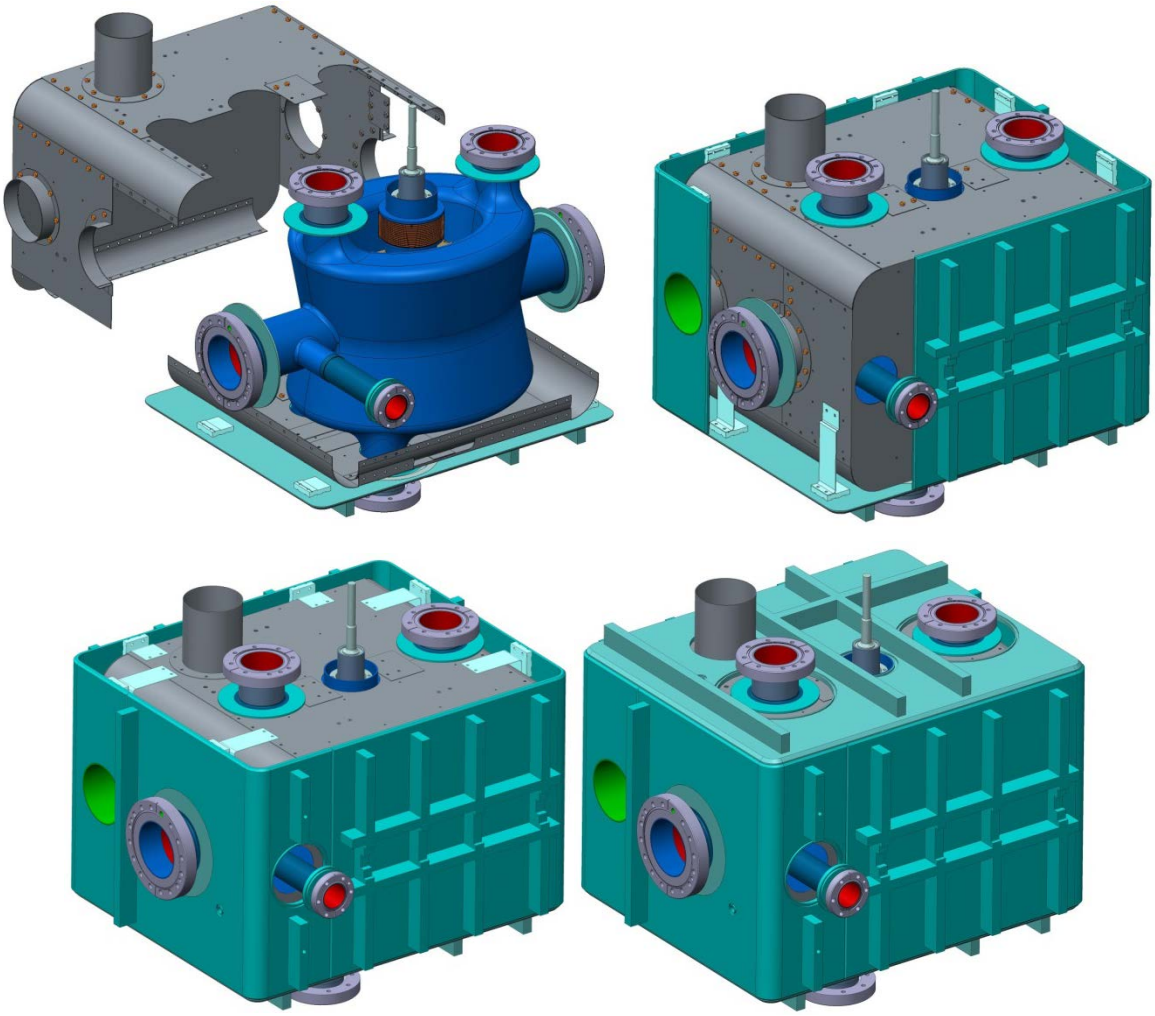

Figure 18: Some stages during the assembly of cold magnetic shield inside the helium vessel

4.5.2. Cold Shield Mechanical Analysis

Magnetization of both materials is adversely affected due to stresses. Hence degradation of the shielding material during assembly and handling should be carefully studied and monitored. Effects of weight and thermal stresses were modelled in ANSYS Figure 19. The simulations indicate that while the maximum stress is 439 MPa in the Ti supports, the stress on the shield is kept to less than 150 MPa. It is possible that this may affect the magnetization locally, but the effect is comparable to that of a small hole in the shield.

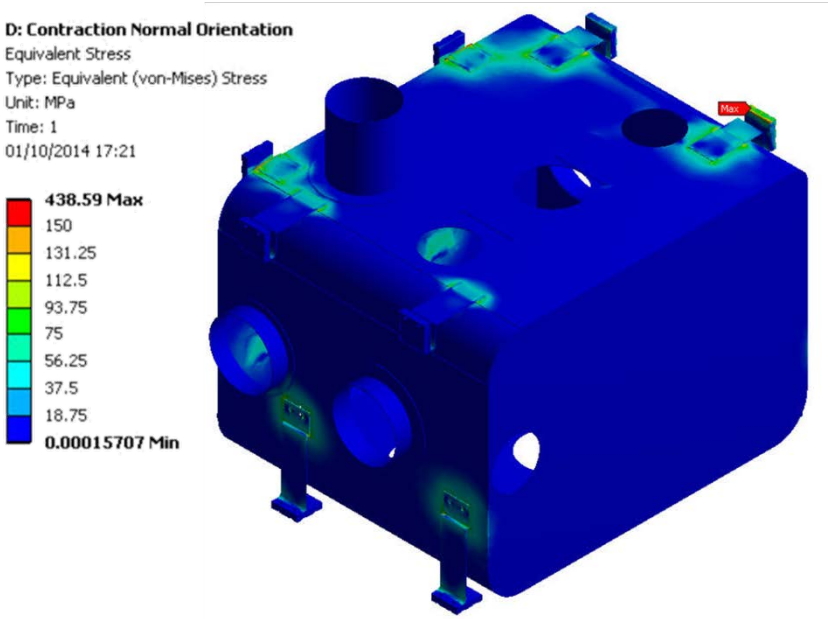

Figure 19: Cooldown and self-weigh stresses in the internal magnetic shield.

4.6. RF COUPLERS AND INTERFACES

4.6.1. Fundamental Power Coupler

The RF power coupler was designed [15] in view of the HL-LHC requirements; additional constraints (common platform) were introduced to limit the variances between the alternative designs in view of the SPS tests.

The crab cavity power coupler adopted will use a single coaxial disk window type to separate the cavity vacuum and the air side. The antenna shape is specific to each cavity as the coupling mechanisms to the different cavities are not identical. However, a common platform starting from the cavity flange followed by the ceramic and double wall tube is imposed. To respect the common platform, the inner antenna is dimensioned to 27 mm diameter with the outer coaxial line of 62 mm diameter for a maximum power capability of approximately 200 kW. The inner line is made of a copper tube and the outer line is Stainless Steel 316LN with inner surface coated with copper. The vacuum to air separation is achieved with a coaxial ceramic window (Al_2O_3) with the outer flange made of titanium. The rest of the items are built from massive OFE 3D forged copper blocks. The coupler body is made of a conical line to increase the near the ceramic region to limit arcing with the primary aim to enlarge the air side to the maximum while keeping the 62/27 mm dimensions for the input antenna in the vacuum side. A coaxial to waveguide transition is performed with a WR2300 half-height without a doorknob (see Figure 20 left).

The air side of the coupler will be air-cooled while the antenna itself will be water-cooled. The waveguide design includes the possibility of a DC polarisation in order to avoid multipacting effects. Each coupler is equipped with three ports for a vacuum gauge, electron monitoring and arc detection devices. The vacuum gauge, mandatory to protect the window during conditioning as well as in operation, will be oriented along the air line in order to minimize the cryomodule flange size. Special test boxes to condition the couplers are also designed (see Figure 20). The Coupler ports are designed to come out on the top,

perpendicular to the beam axis for ease of integration with the WR2300 waveguide transition. The cavity Helium vessel is designed to withstand the weight of the couplers and the waveguide (approx. 35 kg). The alternating crossing angle scheme will require that the orientation of a coupler assembly be robust for horizontal and vertical deflections (Figure 20).

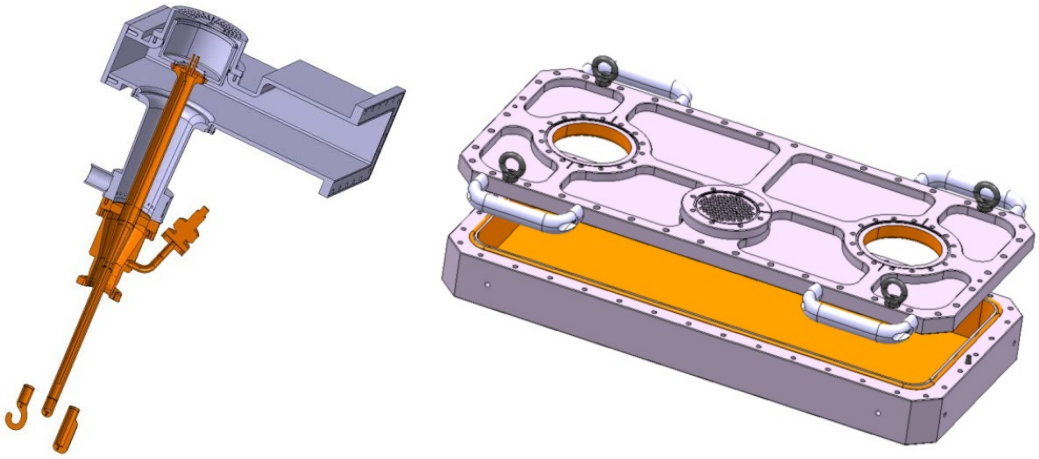

Figure 20: Input coupler assembly (left) and the test box for RF conditioning.

4.6.2. Higher Order Mode Couplers

The first design goal of the HOM filter is to block the transmission of the main deflecting mode, while transmitting all remaining HOMs. Several HOM coupler designs were developed and optimized for different cavity geometries. Two high-pass filter designs, incorporating a notch filter at the fundamental frequency are shown in Figure 21 with both HOMs using hook-like antennas to couple to the HOMs [16].

Simulations show that the HOM coupler must have a superconductive surface due to the high fields of the fundamental mode. A second design constraint requires the HOM couplers to be able to efficiently remove the power in the HOMs (up to 1 kW) and the heat dissipated by the fundamental mode in the inner part of the HOM coupler from the cavity. High purity bulk niobium with sufficient cooling can ensure this. The required cooling may be possible by conduction, but active cooling with superfluid liquid helium in a small LHe tank is adopted for both cavities. For the DQW cavity, additional channel is machined in the inner conductor to further minimize the temperature gradient due to the proximity of the antenna to the high magnetic field region of the deflecting mode.

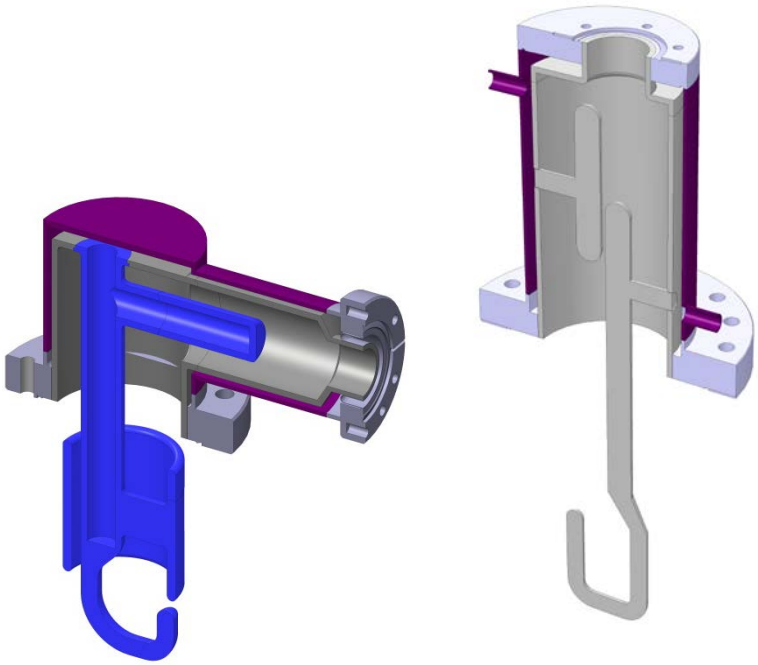

Figure 21: HOM filter for the DQW (left) and RFD (right).

4.6.3. Tuner

The final resonance frequency of the cavity will depend on a number of fabrication and handling steps and cool-down (hundreds of kHz). A "slow" mechanical tuning system is required to compensate for the uncertainties of the above steps by altering the cavity shape – this will dominate the tuner requirement. At 2 K, it must be possible to tune the cavity to $f_{res} = f_{operation} \pm \Delta f_{LFD}$, where Δf_{LFD} denotes Lorentz force detuning occurring during cavity filling. The operating frequency can vary by additional 60 kHz [3]. Despite the large resulting tuning range ($\approx \pm 200$ kHz) the resolution of the tuner should allow at least 4 steps inside the cavity bandwidth ($\approx$ 800 Hz); backlash and hysteresis must be small.

The tuning system, similar for both cavities (DQW and RFD), is shown in Figure 12 and Figure 13. It consists of an actuation system that is placed outside the cryomodule, is operated at room temperature and at atmospheric pressure, which makes it accessible and thus maintainable. The actuation system consists of a stepper motor, a harmonic gearbox, a roller screw and linear guide bearings. The concept is based on a design developed and already in use at JLAB [16]. The detail of the prototype actuation system is shown in Figure 22. Since the cavity will be operated in CW mode and frequency variations are expected to be small, active tuning with piezos may not be needed in the final design. However, the design allows to accommodate a piezo for the first cavity tests to validate if necessary.

The actuation induces a relative movement between two titanium cylinders. The inner one is directly connected to the top of the cavity, the outer one to the bottom via a titanium frame. A symmetric deformation is thus applied simultaneously to the cavity top and bottom.

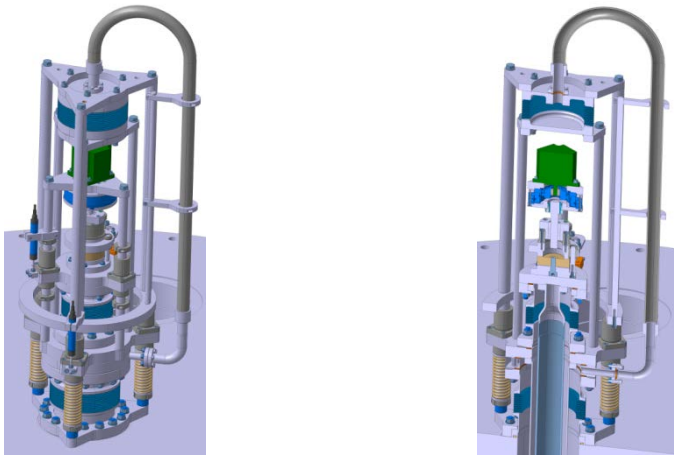

Figure 22: Actuation system of the prototype tuning system for both DQW and RFD cavities.

The estimated mechanical resolution of the tuning at the connection to the cavity is estimated to be in the order of 0.1 μm, which is equivalent to few tens of Hz for both cavities, allowing for at least 10 micro-steps inside the cavity RF frequency bandwidth.

4.7. THERMAL SHIELDS AND INTERCEPTS

In order to reduce the thermal load on the superfluid helium tanks, the crab cavity module will be equipped with an actively cooled thermal shield at the level of about 80 K. It is planned to thermalize the screen with liquid nitrogen, pressurized at 2-3 bar. The screen will be covered with 30 layers of cryogenic multi-layer insulation (MLI). Two schemes are under consideration for the internal cooling circuits. The first shown in the Figure 7 in section 3.1 provides independent control for cooling individual thermal intercepts on the couplers and thermal shield. It also enables the measurement of cooling power requirements for individual component. This solution is presently assumed as a the baseline.

The alternative scheme shown in the Figure 23 utilises a common thermo-siphon for the components is also considered. Both the solutions are fundamentally similar except that the first requires several outlets (interfaces) for the boiled-off nitrogen at several locations whereas the second scheme requires only one common outlet for the all the circuits. This is still work in progress and a most effective option will be worked out in the next design review meeting.

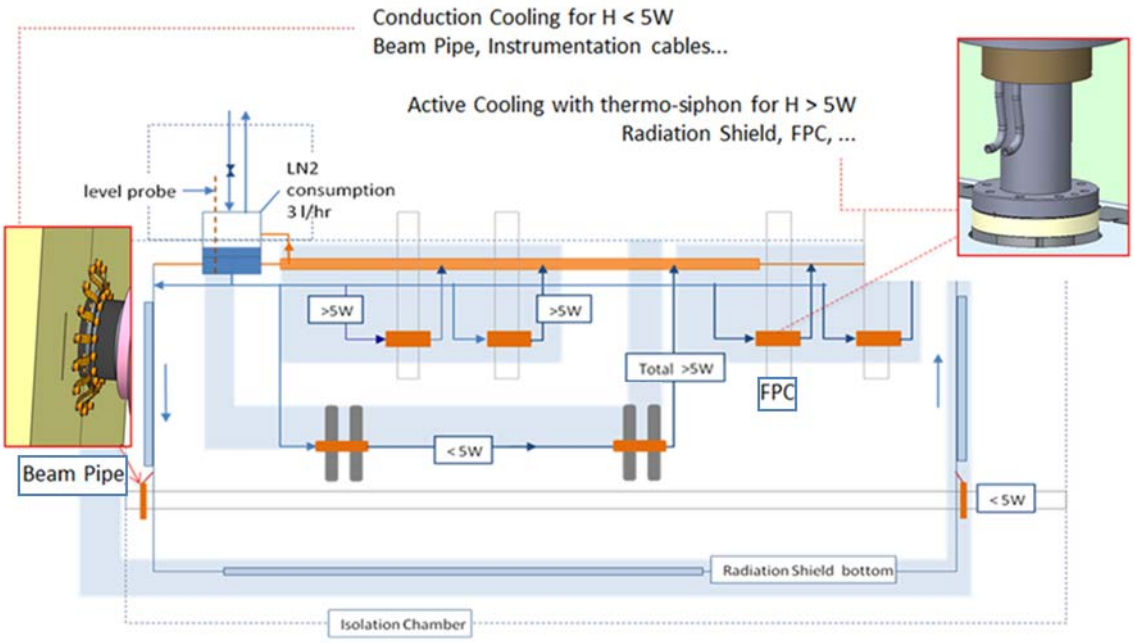

Figure 23: Schematic for 80 K with cooling scheme - 2

4.7.1. Architecture of the Thermal Shield

The thermal shield consists of two window frame sections (including pipes) and four side panel sections. The frame is assembled around the cavity string as shown in Figure 24 and then suspended by flexure mounts (Figure 25) from the OVC. The LN_2 lines are then connected to the cryogenic services port. Each side panel can be removed independently, allowing access to internal components.

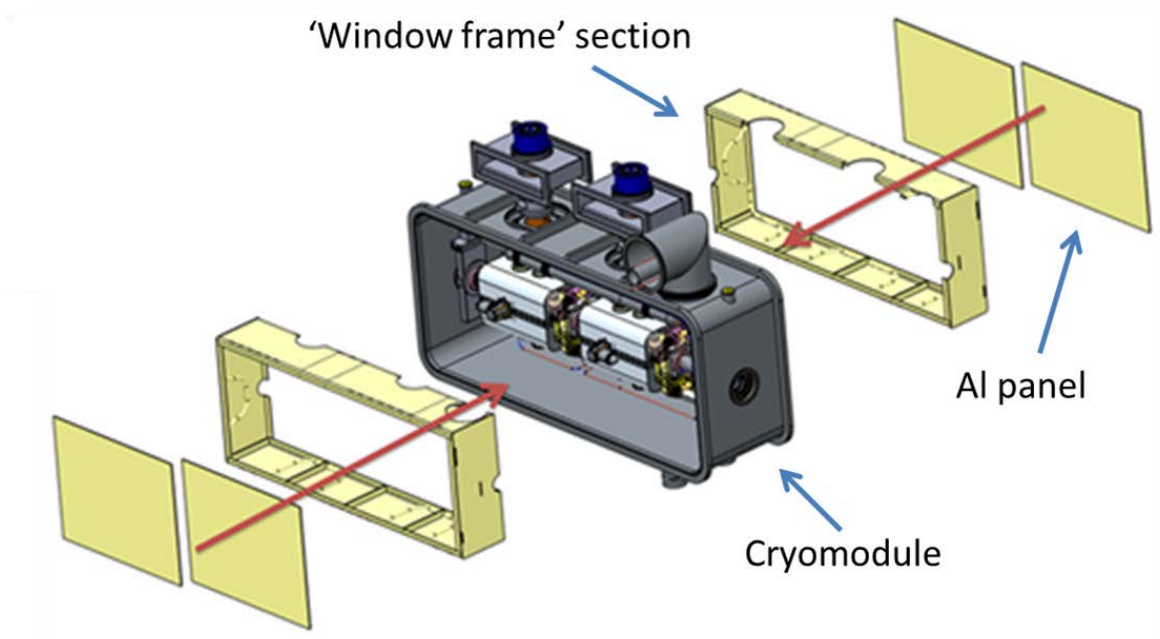

Figure 24: Assembly of the thermal shield inside the cryomodule

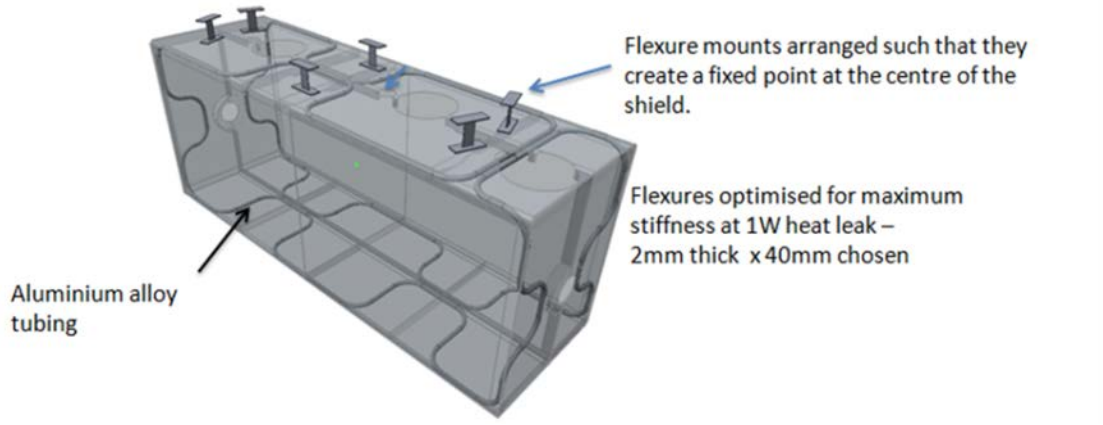

Figure 25: Assembled thermal shield with flexure mounts

4.7.2. Material Selection and Welding Scheme

The shield panels and the pipes are fabricated from Al 6061-T6. The shield is subject to higher stresses during cooldown and hence 6061-T6 has been chosen for its significantly higher yield stress and increased weldability. The shield is suspended from 6 flexure mounts attached to the inside of the OVC. The mounts are arranged such that they create a fixed point at the center of the shield. The results of the thermal and mechanical analysis show how the flexures are allowed to deform as the shield cools. Ti-6Al-4V has been selected for the flexure mounts as used on the SPICE instrumentation support [ref]. The cooling pipes are welded directly to the shield. Al 5356 is used as the filler for welding Al 6061 to itself. By staggering the welds and only welding longitudinally the pipes are allowed to flex during cooldown, reducing stresses in the shield. The pipes are welded through slots in the panels.

4.7.3. Thermal Analysis

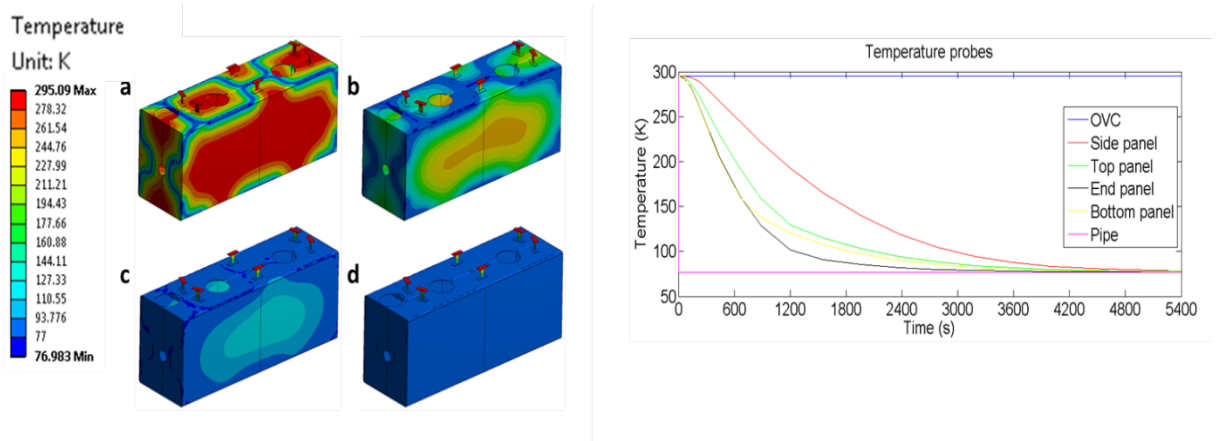

Figure 26: Temperature distribution for fast cool down at (a) t =72 s, (b) t = 588 s, (c) t =2306 s, (d) t = 5400 s ~steady state. The plot on the right shows the temperature profile of components during fast cooldown.

Transient thermal analysis was carried out [18] assuming a fast cooldown (i.e. cooling pipes brought immediately to 77 K) using the boundary conditions given in Table 4. This is considered to be a reasonable assumption for the purposes of mechanical analysis as fast cooldown gives rise to higher thermal gradients (see Figure 26), and hence higher stresses, than will actually be seen by the shield in operation. A margin of safety is therefore introduced into the design through this approach. Figure 26 shows the temperature distribution at various times during fast cooldown of the shield. The flexure mounts are designed to allow heat leak of less than 1 W per flexure in the steady state condition.

Table 4: Transient thermal analysis boundary conditions

Boundary condition	Value(s)	Note
Pipe temperature	T = 77 K	Due to low Re, conduction will dominate heat transfer. Hence, set temperature is a reasonable approximation for the transient model where we assume fast cooldown
Radiation condition	$\varepsilon = 0.011$, T = 300 K	Based on heat flux of 5 Wm^{-2} for compressed MLI (worst case) and view factor consistent with surrounding magnetic shield
Convection to OVC	$h_f = 5\ Wm^{-2}K^{-1}$, T = 300 K	Convection coefficient consistent with free air flow over outer surface of OVC

4.7.4. Structural Analysis

In order to evaluate the worst case stress distribution, the temperature field at the time of highest thermal gradient across the shield was imported as a load into a static structural analysis. A gravitational load is included. Figure 27 (a)-(f) shows the Von Mises stress distributions for the greatest thermal gradient and steady state conditions. The maximum stress that occurs in the worst case is 158.57 MPa in the pipes (allowable limit of 276 MPa), 273.39 MPa in the panels (allowable limit of 276MPa) and 518.55 MPa in the flexures (allowable limit of 880 MPa). The displacements of all points on the shield were also analysed, in order to ensure compatibility with the geometric free space of the cryomodule (Figure 27 (g)-(h)).

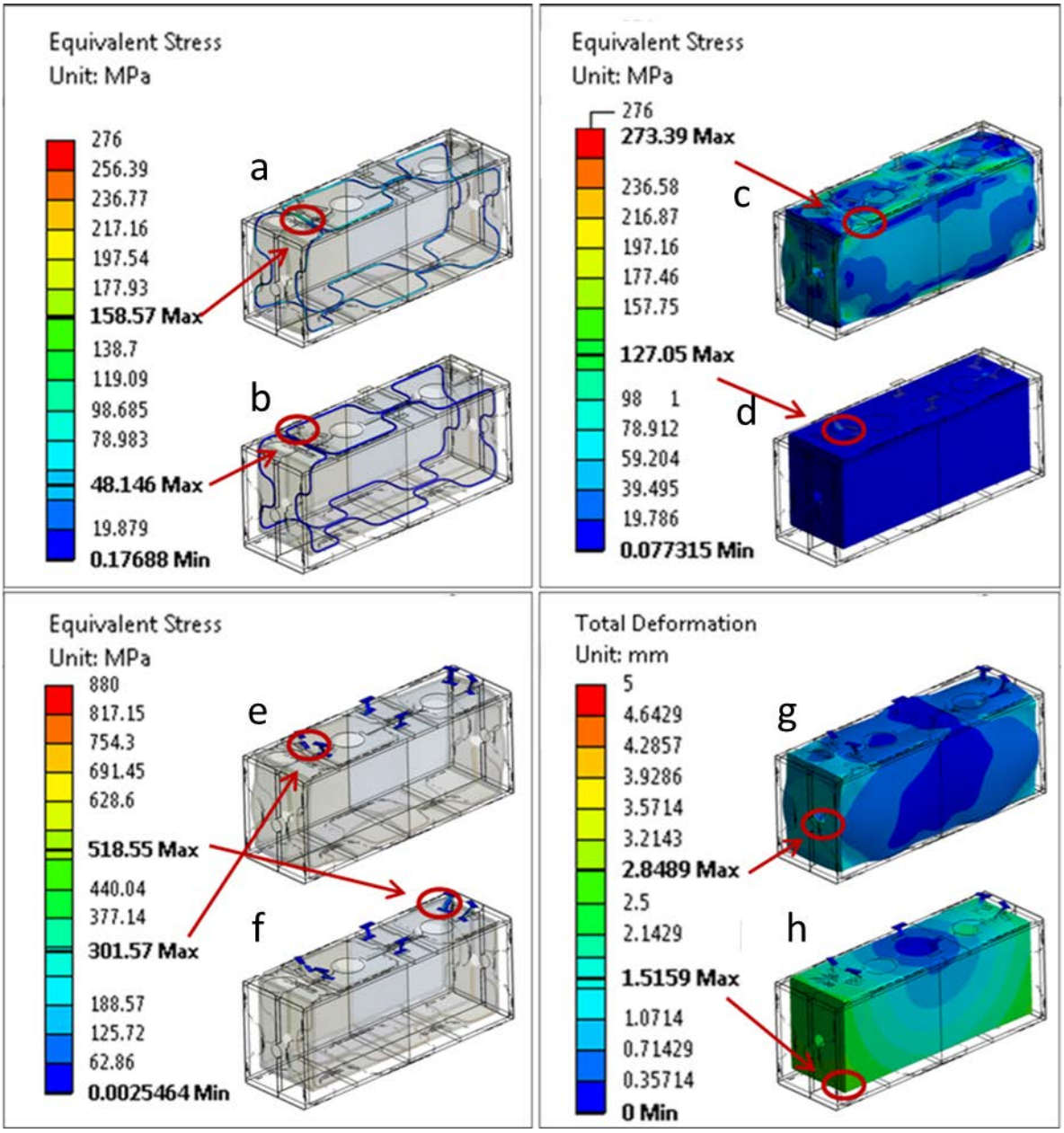

Figure 27 Stress distribution in (a) cooling pipes for maximum thermal gradient across shield, (b) cooling pipes in steady state, (c) shield panels for maximum thermal gradient across shield, (d) the shield panels steady state, (e) flexure mounts for maximum thermal gradient across shield, (f) flexure mounts in steady state and (g) displacement field for shield for maximum thermal gradient, (h) displacement field for shield for steady state

4.8. OUTER VACUUM CHAMBER

4.8.1. Side Loaded Design

The SPS cryomodules [2] are designed to have a rectangular outer vacuum vessel with removable side panels such that the dressed cavities are side-loaded into the vessel. All external connections except the beam pipes are on the top of the cryomodule. The cavities are supported by the power couplers. This allows easy access as required for a prototype. This design requires several stiffening ribs to keep the stress within reasonable limits when placed

under vacuum pressure and during cool-down. The designs for both cavity variants are kept as similar as possible.

A detailed view of the cryomodule containing two DQW and RFD cavities is illustrated in Figure 28. The fixed RF coaxial coupler, with a single ceramic window, providing 80 kW average power, is mounted onto the cavity via a ConFlat™ flange assembly equipped with a specific vacuum/RF seal designed at CERN and widely used elsewhere.

The RF coupler is mounted on the cavity in the clean-room, constraining the assembly of subsequent components of the cryomodule due to its size. The vacuum vessel was designed in three parts and uses a lateral assembly procedure of the cavity string inside the vessel [19]. This allows the possibility of cavity alignment with optical devices (laser trackers for example) while making fine adjustments through the adjustable supports before closing the cryomodule lateral covers.

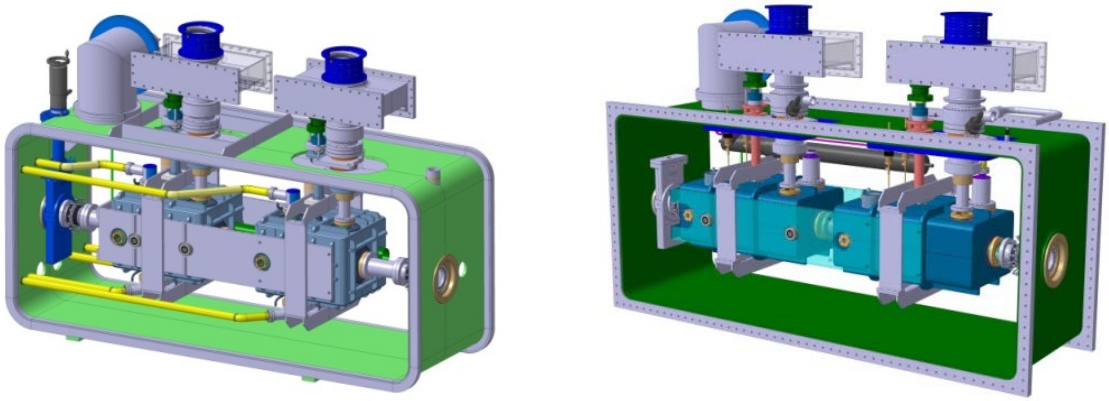

Figure 28: Cryomodules for the DQW (left) and RFD (right) cavities respectively.

4.8.2. Cavity Supports

The cavity supporting concept uses the external conductor of the RF coupler as the main mechanical support of the dressed cavities. An additional supporting point to keep cavity alignment stability within requirements is obtained by the inter-cavity support. In the RFD cavity, the power coupler is transversely offset from the cavity axis, which requires additional vertical support, as shown in Figure 29. Investigations are on-going as to whether such support rods can be used instead of an inter cavity support system. This would give additional space within the module, minimise the mass of the cavity string and allow individual movement of each dressed cavity. Initial analysis shows that using these rods gives a deformation of 0.16mm and maximum stress of 38MPa for the DQW cavity self-weight (shown in Figure 30). Cool down and vibration analyses are ongoing.

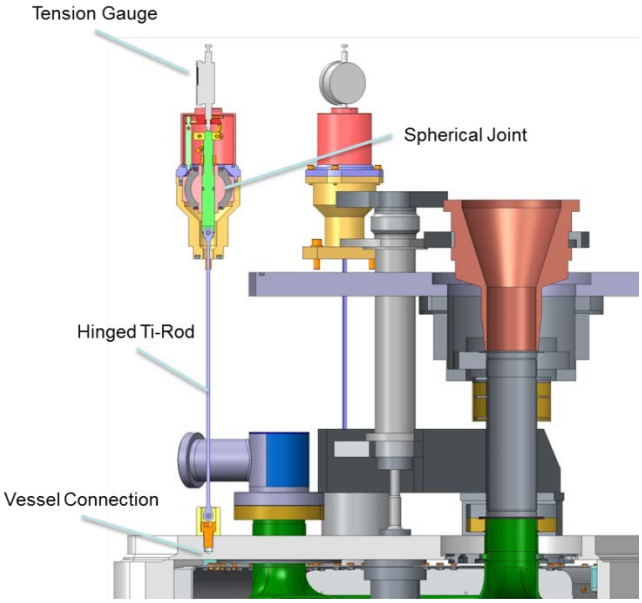

Figure 29 Overview of Cavity support rod

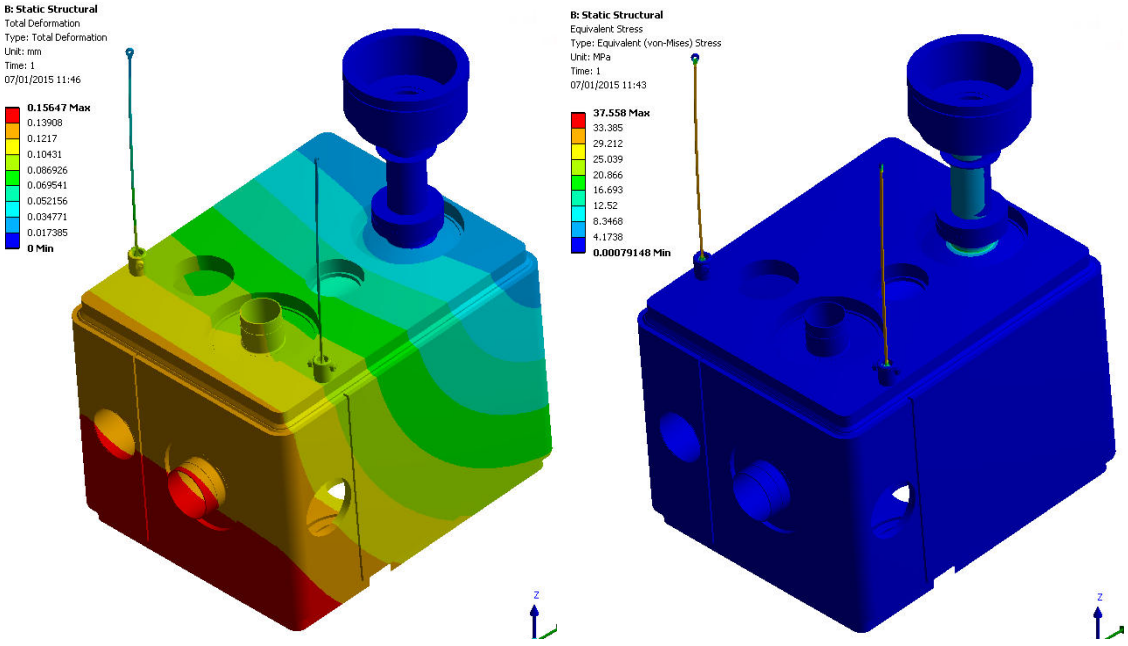

Figure 30: Cavity Support mechanical analysis for dressed cavity self weight.

4.8.3. Mechanical and Thermal Analysis

The design of the OVC has been developed after undertaking thorough mechanical analysis [19] to limit the stress levels within safe limits as shown in the Figure 31.

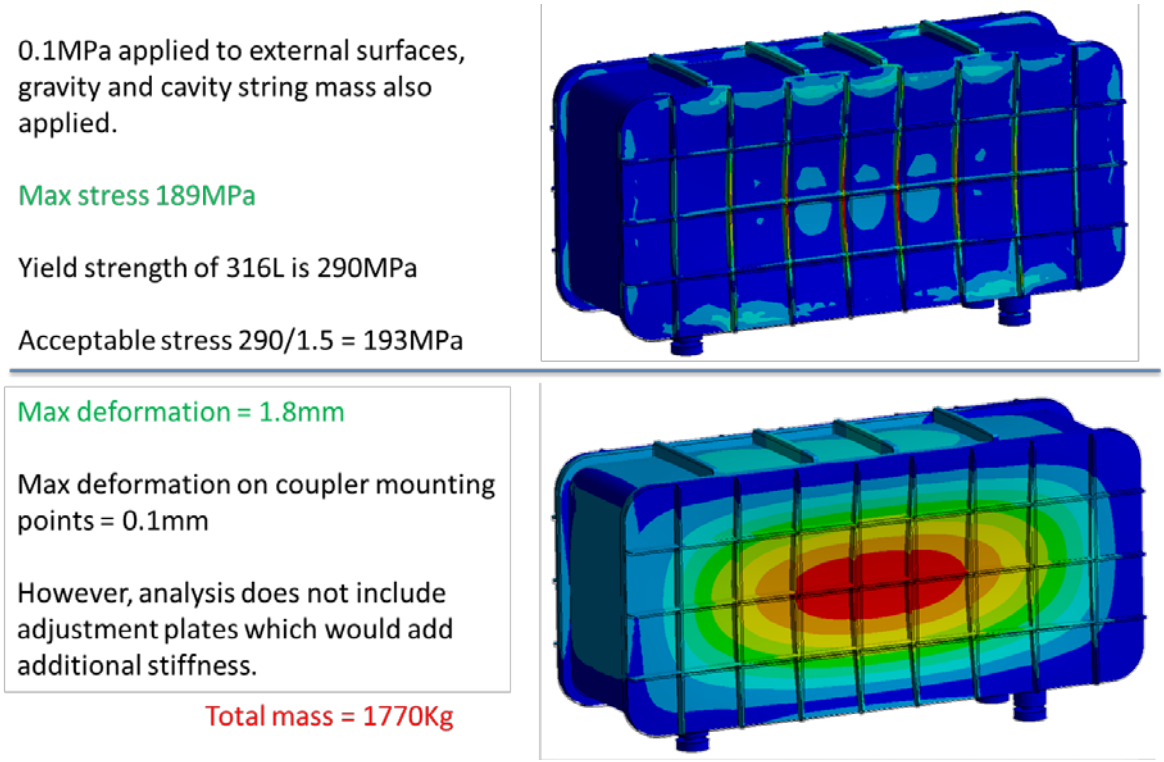

Figure 31: Mechanical analysis of the OVC

5. SCHEDULE

The SPS crab cavity tests are required to be complete prior to the LHC Long Shutdown 2 expected at the end of 2018, as after this date no beam will be available. Two experimental runs are expected one in 2017 and one in 2018. In both runs the cryomodules will be installed during the year end technical stops at the end of 2016 and 2017. For this to occur, cryostating should commence at the beginning of 2016 allowing time for extensive cryomodule testing in SM18 at CERN in mid to late 2016. The overall schedule towards the realisation for HiLumi LHC is shown in the Table 5.

Table 5: Schedule for HiLumi LHC

2013-2014	2015-2016	2017-18	2019-2020	2021-2023	2023-24
Cavity Testing & Prototype Cryomodule design	SPS Cavities & Cryomodule Fabrication	SPS Beam Tests	LHC Pre-series Cryomodule Construction & Testing	LHC series Cryomodule Construction & Testing	LHC Installation

6. SUMMARY

The crab cavity tests in SPS will be the first test of crabbing on a proton beam and will allow testing of many issues that do not affect electron beams, as well as testing the cryomodule designs themselves. As such these tests are critical to the development of crabbing systems for the LHC luminosity upgrade. The cryomodule development is in an advanced state and is near to completion. The dressed cavity designs are now complete including the mechanical design of He II vessel, interfaces, couplers, internal magnetic shielding and tuners. This has allowed the manufacturing of the dressed cavities to commence. Preliminary designs for the outer vacuum chamber, thermal shield and external magnetic shield exist and future work is focussed on developing complete engineering designs for these elements for both cavity designs.

7. REFERENCES

[1] G. Arduini et al., The summary report of the LHC-CC11 workshop, CERN 2011

[2] S. Pattalwar et al., Key Design features of the Crab-Cavity cryomodule for HI-LUMI LHC, in the proceedings of IPAC14, Dresden, 2014.

[3] P. Baudrenghien et al., Functional specification of the LHC prototype crab cavity system, CERN-ACC-Note-2013-003, 2013.

[4] A. Yamamoto et al., Crab cavity system external review report, CERN-ACC-2014-0093, 2014

[5] Q. Wu et al., in the proceedings of IPAC13, Shanghai, 2013

[6] S. De Silva et al., in the proceedings of IPAC13, Shanghai, 2013

[7] A. Macpherson, presented at the Hi-Lumi Annual Meeting, KEK, November 2014

[8] K. Brodzinski, S. Claudet, Hi-Lumi Annual Meeting, KEK, November 2014

[9] K. Brodzinski, et al, crab cavity Engineering meeting, FNAL, December 2012

[10] O. Capatina, Private Communication

[11] O. Capatina, et al., Dressed Crab Cavity Functional Specifications, Crab cavity manufacturing readiness meeting, CERN, 2014

[12] K. Brodzinski, Private Communication

[13] K. Marinov, 'Assessment of the magnetic shielding requirements for Hi Lumi crab Cavities, Hi-Lumi progress review meeting, STFC Daresbury, August 2014

[14] T. Jones et al., Crab cavity manufacturing readiness meeting, CERN, 2014

[15] E. Montesinos, RF Power coupler for Crab cavities, CC-13, CERN , Dec 2013

[16] Z. Li, Crab cavity coupler design update, 4th Joint HiLumi LHC-LARP Annual Meeting 2014

[17] G. Davis et al, Development and testing of a prototype tuner for the CEBAF upgrade cryomodule, PAC 2001

[18] A. J. May et al., et al, Thermal and mechanical analysis of the radiation shield design for Hi-Lumi LHC crab cavity cryomodule, proceedings of ICEC-25, Twente, July 2014

[19] T. Jones, CC Design Review meeting, CERN, August 2013.

ANNEX: GLOSSARY

Acronym	Definition
ACF	Superconducting Crab Cavity
CM	Cryomodule
IP	Interaction Point
IR	Interaction Region
LEP	Large Electron-Positron Collider
LHC	Large Hadron Collider
RFD	RF Dipole Cavity
DQW	Double Quarter Wave cavity